PNAS RESEARCH ARTICLE | NEUROSCIENCE OPEN ACCESS

The mechanosensitive ion channel Piezo1 contributes to ultrasound neuromodulation

Jiejun Zhu[a,b,1], Quanxiang Xian[a,1], Xuandi Hou[a,1], Kin Fung Wong[a], Tingting Zhu[b], Zihao Chen[b], Dongming He[b], Shashwati Kala[a], Suresh Murugappan[a], Jianing Jing[a], Yong Wu[a], Xinyi Zhao[a], Danni Li[a], Jinghui Guo[a], Zhihai Qiu[a,b,2], and Lei Sun[a,2]

Edited by Hee-Sup Shin, Institute for Basic Science, Daejeon, Korea (South); received January 13, 2023; accepted February 27, 2023

Transcranial low-intensity ultrasound is a promising neuromodulation modality, with the advantages of noninvasiveness, deep penetration, and high spatiotemporal accuracy. However, the underlying biological mechanism of ultrasonic neuromodulation remains unclear, hindering the development of efficacious treatments. Here, the well-known Piezo1 was studied through a conditional knockout mouse model as a major mediator for ultrasound neuromodulation ex vivo and in vivo. We showed that Piezo1 knockout (P1KO) in the right motor cortex of mice significantly reduced ultrasound-induced neuronal calcium responses, limb movement, and muscle electromyogram (EMG) responses. We also detected higher Piezo1 expression in the central amygdala (CEA), which was found to be more sensitive to ultrasound stimulation than the cortex was. Knocking out the Piezo1 in CEA neurons showed a significant reduction of response under ultrasound stimulation, while knocking out astrocytic Piezo1 showed no-obvious changes in neuronal responses. Additionally, we excluded an auditory confound by monitoring auditory cortical activation and using smooth waveform ultrasound with randomized parameters to stimulate P1KO ipsilateral and contralateral regions of the same brain and recording evoked movement in the corresponding limb. Thus, we demonstrate that Piezo1 is functionally expressed in different brain regions and that it is an important mediator of ultrasound neuromodulation in the brain, laying the ground for further mechanistic studies of ultrasound.

transcranial ultrasound neuromodulation | focused ultrasound | mechanosensitive ion channels | Piezo1 | sonogenetics

Significance

Ultrasound has emerged as a promising neuromodulation technique because of its noninvasiveness, deep penetration, high spatiotemporal accuracy, and excellent safety. However, its underlying biological mechanism remains unclear, which hinders its clinical potential and further development to be fully utilized. In this study, we find that mechanosensitive ion channel Piezo1 is a major mediator responsible for the neuromodulatory effect of ultrasound to regulate neuronal signaling and animal behaviors. This paves the way for the development of more effective and targeted ultrasound-based neuromodulation strategies and may offer a broad avenue for the treatment of a range of neurological and psychiatric disorders.

Ultrasound is an emerging technology capable of noninvasively modulating neurons in various brain regions, whether relatively deep or superficial, with minute spatial and temporal resolution. Multiple studies have demonstrated effective ultrasonic activation of the human cortical (1, 2), subcortical (3), and related networks (1–5). Basic clinical trials with ultrasound have shown improvement in specific behavioral outcomes, such as improved mood (6, 7) and increased responsiveness in patients with chronic disorder of consciousness (8). Crucially, there were no observable side effects in these studies even with chronic stimulation. Multiple studies have also shown that ultrasound stimulation of specific neurons or brain regions can elicit distinct behaviors, such as motor or visuomotor response, in rodents (9–15), sheep (16), and monkeys (17, 18). Thus, a growing body of evidence shows ultrasound to be a promising neuromodulation modality—generally safe, deliverable noninvasively, and apt for clinical translation. However, the biological mechanism underlying the neuromodulatory effects of ultrasound remains to be elucidated. This lack of clarity is a hurdle in the path of future ultrasound-based therapies if they are to be applied predictably and consistently, with maximal achievable efficacy and minimal side effects.

Ultrasound comprises acoustic waves at frequencies above the upper limit of the audible range for humans (20 kHz). When exposed to ultrasound, nanometer-scale compression and particle displacement of the medium occurs, with heat, cavitation, or acoustic radiation force (ARF) generated when the particles return to their original configurations. Depending on the energy level, ultrasound can be categorized as high or low intensity (19). High-intensity ultrasound produces heat, and this has been used to develop high-intensity focused ultrasound (spatial-peak temporal average intensity, ISPTA > 1,000 W/cm^2). This has been applied as a treatment for several neurological diseases including essential tremor (20), Parkinson's disease (21), and obsessive-compulsive disorder (22). However, ultrasound that can modulate neurons without cell damage would require low intensity (ISPTA < 500 mW/cm^2), where the induced temperature change would be minor (<0.1 °C) (19, 23–27). Furthermore, mutant *C. elegans* worms with and without knockout of thermosensitive ion channels showed no difference in neuronal response to low-intensity ultrasound stimulation (28), implying a mechanical, rather than

Author contributions: J.Z., J.G., Z.Q., and L.S. designed research; J.Z., Q.X., X.H., K.F.W., T.Z., D.H., S.K., S.M., J.J., Y.W., X.Z., D.L., and Z.Q. performed research; J.Z., K.F.W., Z.C., S.M., and Z.Q. contributed new reagents/analytic tools; J.Z., Q.X., X.H., K.F.W., S.M., and Z.Q. analyzed data; and J.Z., S.K., Z.Q., and L.S. wrote the paper.

The authors declare no competing interest.

This article is a PNAS Direct Submission.

[1]J.Z., Q.X., and X.H. contributed equally to this work.

[2]To whom correspondence may be addressed. Email: qiuzhihai@gdiist.cn or lei.sun@polyu.edu.hk.

This article contains supporting information online at https://www.pnas.org/lookup/suppl/doi:10.1073/pnas.2300291120/-/DCSupplemental.

Published April 25, 2023.

thermal, mechanism. While cavitation may be induced at higher intensities (29), research using lower intensities showed that micron-scale tissue displacement-induced spiking activity remained unchanged within a broad range of acoustic frequency (0.5 to 43 MHz) (30), suggesting ARF as the dominant physical mechanism.

A pivotal component for cellular sensation of mechanical disturbances like ARF and enablers of fast neuromodulatory effects, mechanosensitive ion channels are plausible mediators of ultrasound (27, 31). Studies have shown ultrasound to be significantly more effective in cells overexpressing one of various such channels in vitro (32–35), in a simple nervous system (28) and in animals (36). Ultrasound was also found to be capable of indirect neuromodulation through activating astrocytic TRPA1, a member of the transient receptor potential (TRP) family (37). These results suggest that the ultrasonic effect in the mammalian brain could be modulated by endogenous mechanosensitive ion channels that are present. Piezo1, the most sensitive mechanotransduction ion channel, is known to respond to force as low as 10 pN (38, 39). Separately, hippocampal neurons have been shown capable of sensing localized mechanical force as low as 13 to 50 pN (40). Interestingly, online databases (41, 42) show broad expression of Piezo1 RNA across both the human and mouse brains. Taken together, these facts led us to hypothesize that Piezo1 could be mediating the neuromodulatory effects of ultrasound in vivo.

Our previous study showed the significant contribution of Piezo1 in the ultrasonic stimulation of neurons in vitro (33). We thus wanted to investigate the role of Piezo1 in live animals in the present study. We first determined the functional expression of Piezo1 in the mouse brain with the generation of Piezo1 knockout (P1KO) neurons. The functional expression of Piezo1 and the success of conditional knockout were confirmed by genotyping, immunostaining, and calcium imaging with the Piezo1 agonist Yoda1. We then tested the neuronal activity induced by ultrasound both ex vivo and in vivo. In acute brain slices, ultrasound-induced calcium influx was significantly reduced in P1KO neurons and in neurons pretreated with the broad mechanosensitive ion channel blocker ruthenium red (RR) (43) compared to those with functional Piezo1. We also used in vivo motor responses as a gauge of ultrasound stimulation as in previous studies (14, 44). P1KO mice displayed lowered responses to ultrasound stimuli in the motor cortex, measured by reduced contralateral limb movement, reduced muscle EMG responses, and reduced calcium signaling and c-Fos expression. Further, in a brain region showing higher Piezo1 expression than the cortex, neurons showed greater sensitivity to ultrasound stimulation as well. Taken together, our loss-of-function and agonist-stimulated experiments demonstrate Piezo1 as a major mediator of ultrasonic neuromodulation in vivo. We also excluded an auditory confound by monitoring c-Fos expression in the auditory cortices of control, P1KO, and deafened mice. In short, the present study demonstrates that Piezo1 is a key mediator for ultrasonic neuromodulation in the mouse brain and provides a basic study of its spatial distribution in different brain regions.

Results

Piezo1 Mediates Neuronal Responses to Ultrasound Stimuli in Ex Vivo Brain Slices. We first examined whether Piezo1 was expressed endogenously at a sufficiently high level to be functionally detected. Previous studies have used neurons of the mouse cortex for in vitro studies (33, 35) as well as for in vivo motor cortex stimulation (9, 13, 14). Hence, we opted to build upon this literature by testing Piezo1's possible contribution to ultrasound neuromodulation in the mouse cortex. We found cortical cells coexpressing PIEZO1 and MAP2 (Fig. 1*A*), confirming the expression of Piezo1 in cortical neurons. The Piezo1 antibody's specificity was verified by confirming a loss of observed staining when brain tissue was preincubated with the antibody's specific blocking peptide (*SI Appendix*, Fig. S1). We also found neurons costained for GFAP (Glial fibrillary acidic protein, an astrocytic marker) and PIEZO1, indicating the expression of Piezo1 in astrocytes as well (*SI Appendix*, Fig. S2).

To evaluate the role of Piezo1 in ultrasound neuromodulation, mice with conditional knockout of Piezo1 in neurons of the cortex were generated using the Cre-LoxP system (Fig. 1*B*). Mice with exons 20 to 23 of Piezo1 flanked by LoxP sites (45) were bred, and the Cre recombinase-mCherry virus was delivered to the cortex by local injection, thus generating mice with P1KO in cortical neurons (Fig. 1*B*). A virus coding for mCherry alone was used as a control (Ctrl). PCR genotyping with primers spanning the deletion showed the expected pattern (45), with a 230-bp band seen exclusively in P1KO mice (Fig. 1*C*), indicating a successful P1KO model. Immunostaining for Piezo1 showed much reduced fluorescent signals in P1KO neurons compared to Ctrl (Fig. 1*D* and Movies S1 and S2), confirming the knockout of Piezo1 in neurons of the targeted region.

The functioning of endogenous Piezo1 was then tested by calcium imaging, using a pharmacological agonist or antagonist and ultrasound stimulation. An additional virus encoding the genetically encoded calcium sensor GCaMP6s was delivered along with Cre-mCherry or mCherry viruses. This generated P1KO and Ctrl mice with GCaMP6s neuronal expression in their motor cortices. Acute brain slices were collected 4 wk postinjection and treated with Yoda1 or ultrasound, in a setup building by a 0.5-MHz plane transducer, a gassed perfusion system, and an inverted fluorescent microscope (*SI Appendix*, Fig. S3). Calcium influxes were observed when Ctrl brain slices were treated with 20 μM of the Piezo1 agonist Yoda1 ($\Delta F/F$ = 60.36% ± 43.92%), but this was significantly reduced in the RR+Yoda1 condition (14.27% ± 17.26%) and in P1KO neurons treated with Yoda1 (46.88% ± 54.95%) (Fig. 1 *E*–*G*). Neurons in the acute brain slices were then treated with the pulses of ultrasound (US) at 0.35 MPa with 1-kHz PRF, 50% duty cycle, for 300 ms, to test their ability to respond to ultrasound stimuli. Consistent with the Yoda1 pattern, Ctrl neurons showed a significantly stronger calcium response to ultrasound sonication (115.3% ± 147.8%) than Ctrl + RR (83.83% ± 146.2%) or P1KO neurons (38.65% ± 38.27%) ((Fig. 1 *H*–*J*), and there is no significant difference between the latter two groups' responses. These imaging data confirm the functional expression of Piezo1 channels in the given regions as well as the neurons' ability to respond to the mechanical stimulus of ultrasound and the reduced Piezo1 expression in P1KO mice. Taken together, we found that Piezo1 was functionally expressed in cortical neurons of mouse brains, and it was an important mediator for ultrasound neuromodulation in ex vivo brain slices.

Cortical Piezo1 Is an Important Mediator for Ultrasound-Induced Motor Behavior In Vivo. We further studied evoked motor responses to evaluate the role of Piezo1 in ultrasound neuromodulation at the behavioral level. In P1KO or Ctrl mice, ultrasound stimuli of varying intensities were delivered to the right motor cortex, and responses in the left forelimb and hind limb were monitored using a high-speed camera and EMG measurement (Fig. 2 *A* and *B*). Ultrasound applied was of 0.5-MHz frequency, 1-kHz PRF, 50% duty cycle. Consistent with previous studies, contralateral limb movement and EMG signal could be induced by ultrasound stimulation (14, 44). In both Ctrl and P1KO mice, forelimb movement was found to increase

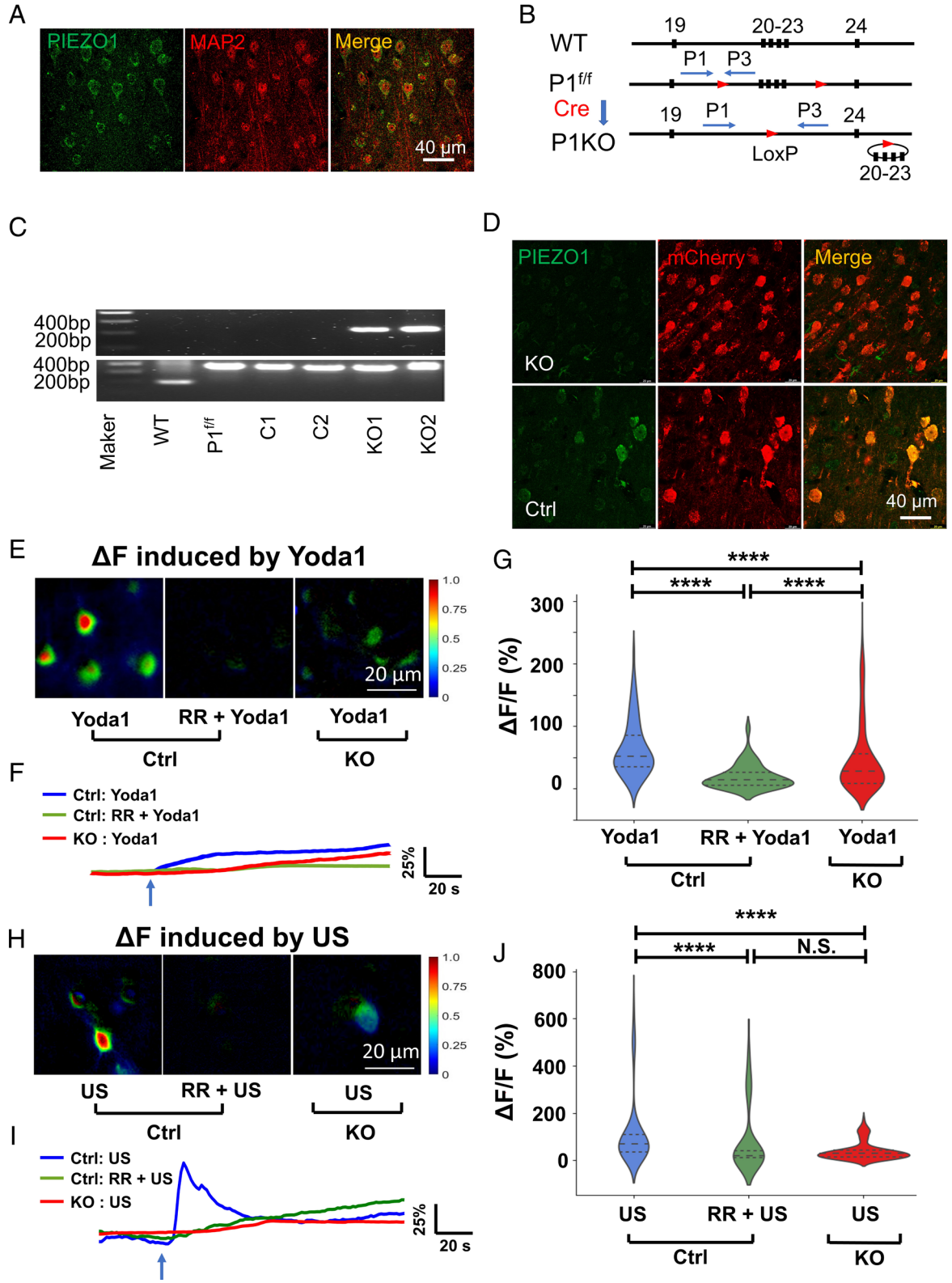

Fig. 1. Piezo1 contributes to neuronal responses to ultrasound stimuli in ex vivo brain slices. (*A*) Immunostaining of Piezo1 and MAP2 of the cortex of wild-type (WT) mice. (*B*) Schematic illustration of Piezo1 conditional knockout by the Cre-LoxP system. (*C*) *Top*: Genotyping results with deletion-spanning PCR primers. The expected PCR product size is 230 bp after deletion and 3,080 bp without deletion which cannot be amplified; *Bottom*: Genotyping results with LoxP-spanning PCR primers. Expected size in Piezo1$^{f/f}$ mice = 380 bp, WT = 188 bp. (*D*) Immunostaining of Piezo1 in Ctrl and P1KO mice brains. (*E*) Representative images of ex vivo neuronal calcium signaling from brain slices of Ctrl or P1KO mice after adding 20 μM Yoda1. (*F*) Representative calcium traces of one neuron from brain slices of Ctrl, Ctrl+RR, or P1KO mice after adding 20 μM Yoda1. (*G*) Summarized calcium changes of neurons from ex vivo experiments. n is as follows: 208 neurons from four Ctrl mice; 66 neurons from four Ctrl mice + RR; 316 neurons from five P1KO mice. Bars represent the median and interquartile range; ****P < 0.0001, by one-way ANOVA with post hoc Dunn's test. (*H*) Representative images of ex vivo neuronal calcium signaling from brain slices of Ctrl or P1KO mice treated with 0.35-Mpa US. (*I*) Representative calcium traces of one neuron from brain slices of Ctrl, Ctrl+RR, or P1KO mice treated with 0.35-MPa US stimulation. (*J*) Summarized calcium changes from ex vivo experiments. n is as follows: 277 neurons from four Ctrl mice; 98 neurons from four Ctrl mice + RR; 283 neurons from five KO mice. Bars represent the medium and interquartile range; ****P < 0.0001; N.S., not significant, by one-way ANOVA with post hoc Dunn's test.

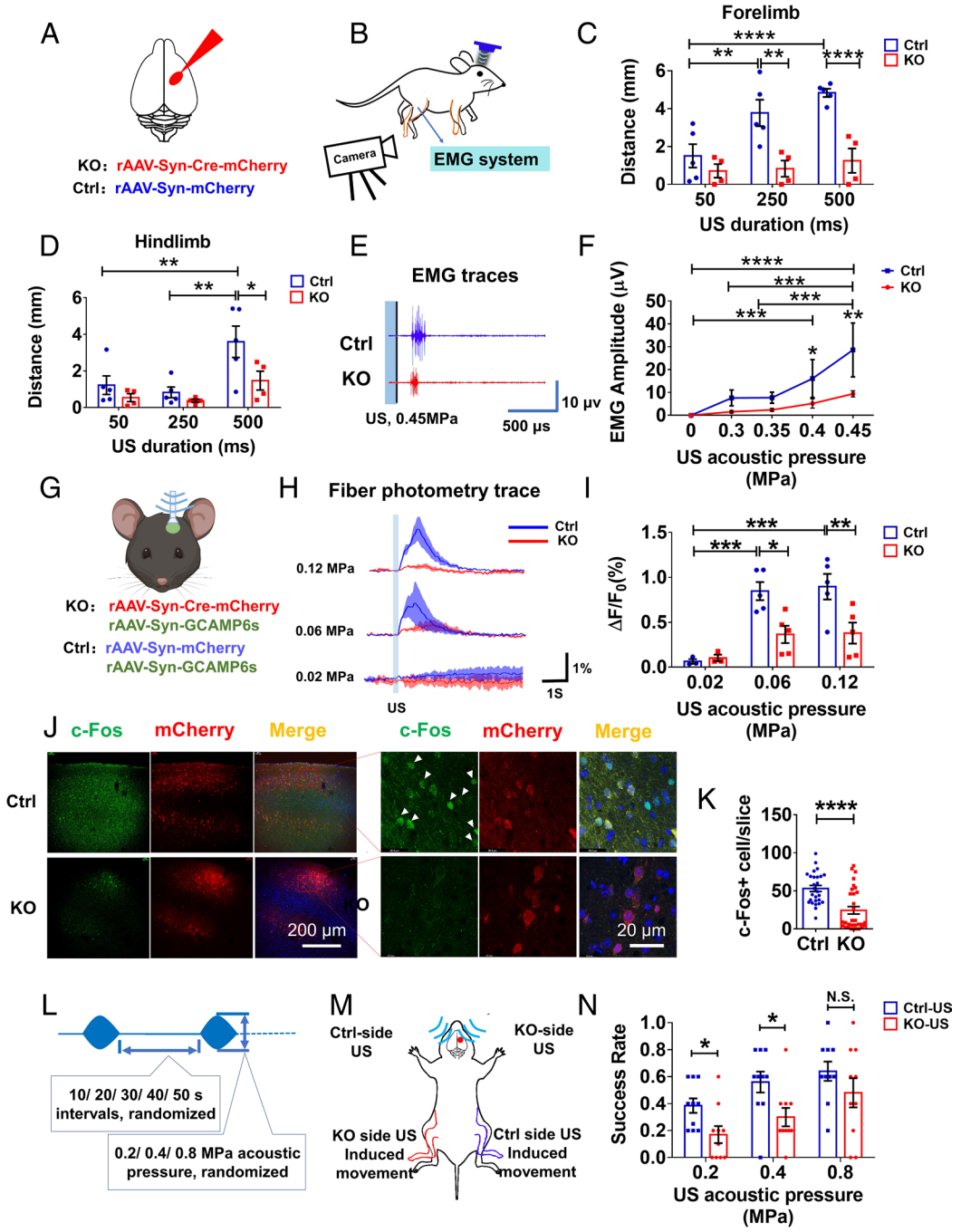

Fig. 2. Cortical Piezo1 is an important mediator for ultrasound-induced motor behavior in vivo. (*A*) Schematic illustration of virus injections into the mouse cortex for obtaining Ctrl and P1KO mice. (*B*) The right motor cortex of Ctrl or KO mice was treated with ultrasound stimuli at different parameters, and responses in the left forelimb and hind limb were monitored with a high-speed camera and EMG measurement. (*C*) Summarized forelimb movement upon ultrasound stimulation. N = 5 for Ctrl and 4 for P1KO mice. Bars represent mean ± SEM; $^{*}P < 0.05$ and $^{**}P < 0.01$ by two-way ANOVA followed by Sidak's test. Ultrasound parameters were as follows: frequency: 0.5 MHz, PRF: 1kHz; amplitude: 0.35 MPa, duty cycle: 50%; 5-s intervals, 6 to 10 times repetition for each US duration. (*D*) Summarized hind limb movement at varying ultrasound stimulation durations. N = 5 for Ctrl and 4 for P1KO mice. Bars represent mean ± SEM, $^{*}P < 0.05$ by two-way ANOVA followed with post hoc Sidak's test for group factor and Tukey's test for duration factor. Ultrasound parameters were as follows: frequency: 0.5 MHz, PRF: 1 kHz, amplitude: 0.45 MPa; duty cycle: 50%; 5-s intervals, 6 to 10 times repetition in each US duration. (*E*) Representative EMG traces induced by ultrasound stimulation in Ctrl (*Top*) and P1KO (*Bottom*) mice. (*F*) Summarized EMG result at varying acoustic pressures. The ultrasound parameters were as follows: frequency: 0.5MHz, duty cycle: 50%, duration: 500 ms, 15-s intervals, four to six times repetition for each group. n = 5 for Ctrl and 4 for P1KO mice. Bars represent the mean ± SEM, $^{*}P < 0.05$, $^{**}P < 0.01$, $^{***}P < 0.001$, and $^{****}P < 0.0001$ by two-way ANOVA followed by Tukey's test. (*G*) Schematic illustration of virus injections for fiber photometry in Ctrl and KO mice. (*H*) Representative calcium signaling traces induced by ultrasound stimulation in Ctrl (*Top*) and P1KO (*Bottom*) mice at different acoustic intensities. (*I*) Summarized calcium signals induced by ultrasound stimulation in five Ctrl mice and five P1KO mice. Bars represent mean ± SEM; $^{*}P < 0.05$, $^{**}P < 0.01$, and $^{***}P < 0.001$ by two-way ANOVA with post hoc Sidak's test. (*J*) Immunostaining of c-Fos in the motor cortex of Ctrl and P1KO mice after 0.45-MPa US stimulation for 50 min. *Left*: Low magnification images. *Right*: Zoomed-in images at high magnification. Blue: DAPI, green: c-Fos, red: m-Cherry. (*K*) c-Fos^{+} cells in 27 slices from three Ctrl mice, and 31 slices from three P1KO mice. Bars represent mean ± SEM, $^{****}P < 0.0001$ by an unpaired *t* test. (*L*) Schematic illustration of the ultrasound stimulation parameter for the motor behavioral test. Smoothed-waveform ultrasound was used, amplitude: 0.2/0.4/0.8 MPa; duty cycle: 50%; PRF: 1 kHz; duration: 500 ms; pulse interval: 10/20/30/40/50s. Every pulse was triggered randomly. (*M*) Schematic illustration of the motor behavioral test with ultrasound stimulation either on the virus injection side or the contralateral side. Limb movement in response to each US pulse delivered was recorded using a camera (*N*) Summarized mouse hind limb movement at varying acoustic intensities. N = 5; bars represent the mean ± SEM, $^{*}P < 0.05$ by two-way ANOVA followed by Sidak's test. Ultrasound parameters were as follows: frequency: 0.5MHz; PRF: 1 kHz; amplitude: 0.2/0.4/0.8 MPa; duty cycle: 50%; duration: 500 ms; each pulse was triggered randomly at 10/20/30/40/50s intervals.

with the pulse duration under 0.35-MPa ultrasound (Fig. 2*C*). However, the movement distance in P1KO was significantly lower than in Ctrl mice at 250-ms (0.83 ± 0.74 mm vs. 3.78 ± 1.40 mm) and 500-ms (1.25 ± 1.12 mm vs. 4.84 ± 0.44 mm) pulse durations (Fig. 2*C*). The hind limb showed a similar pattern but a better response to a higher ultrasound intensity, 0.45 MPa (Fig. 2*C*). Nevertheless, the movement induced under these parameters was significantly lower in P1KO mice than in Ctrl mice (1.47 ± 0.90 mm vs. 3.59 ± 1.72 mm; Fig. 2*C*) (Movies S3–S5). EMG responses in P1KO mice were obviously diminished, although not abrogated, compared to the Ctrl (Fig. 2*E*). Upon quantifying EMG amplitude, we found that the response in both Ctrl and P1KO mice increased with growing ultrasound intensities, and the responses in P1KO mice were lower than the Ctrl at every intensity tested (Fig. 2*F*).

To directly measure neuronal activity, we used fiber photometry to record calcium signal changes in P1KO and Ctrl mice expressing GCaMP6s (Fig. 2*G* and *SI Appendix*, Fig. S4). Ultrasound at 0.5-MHz frequency, 1-kHz PRF, 50% duty cycle, 300-ms duration, and acoustic pressures between 0.02 to 0.12 MPa were used to stimulate the brains. We found that ultrasound rapidly and transiently activated neurons, as measured by GCaMP6s fluorescence change, at all tested acoustic pressures, and this response was also found to increase with acoustic pressure (Fig. 2*H*). However, responses from P1KO cells were significantly lower than the Ctrl (Fig. 2 *H* and *I*).

Aside from real-time responses, the expression of the activation marker c-Fos was also evaluated as a poststimulation measure of neuronal activity (Fig. 2*J*). Compared to Ctrl mice, P1KO mice showed a significantly reduced c-Fos levels (24.32 ± 27.00 vs. 53.04 ± 20.40; Fig. 2 *J* and *K*). We also monitored c-Fos expression in auditory cortices of these mice to evaluate the known auditory confound effect, known to be a possibility with ultrasonic neuromodulation (46, 47). No obvious differences were found between Ctrl and P1KO mice (90.36 ± 17.41 vs. 93.36 ± 34.21, *SI Appendix*, Fig. S5), indicating a low chance of auditory effects being the cause of the observed behavioral differences.

To further exclude the possible auditory confound, we perform ultrasound stimulation on the P1KO site and their contralateral site by using smoothed waveforms while observing the contralateral responses (48). The ultrasound stimulation is triggered randomly to diminish the accumulated effect of the previous stimulations (Fig. 2*L*). Then, five P1KO mice were prepared as before and treated with the ultrasound stimulation at either the ipsilateral hemisphere (where the virus is injected, KO side) or the contralateral (contralateral side of virus injection, Ctrl side) (Fig. 2*M*). The success rate of the contralateral limb movement under each ultrasound pulse was measured. We found that the KO-side ultrasound stimulation showed a lower successes rate in inducing the limb movement in mice especially under the 0.2-MPa (0.37 ± 0.16 vs. 0.18 ± 0.18) and 0.4-MPa (0.54 ± 0.23 vs. 0.27 ± 0.21) ultrasound stimulations (Fig. 3*N*). In addition, this phenomenon is dismissed when ultrasound intensity reached 0.8 MPa, which may indicate an alternative mechanism under higher-intensity ultrasound neuromodulation. These results confirm that Piezo1 contributes to ultrasound neuromodulation specifically rather than auditory confound.

Neuronal Sensitivity to Ultrasound Stimuli Is Dependent upon the Presence of Neuronal Piezo1. Having found endogenous Piezo1 to be an important contributor to ultrasound neuromodulation in the motor cortex, we were led to wonder whether other brain regions, possibly expressing greater levels of Piezo1, may also serve as effective targets of ultrasound. We performed immunofluorescent staining of WT mouse brains and found several brain areas with strong Piezo1 expression, including the central amygdala (CEA), bed nucleus of the stria terminalis (BNST), paraventricular nucleus of the hypothalamus (PVN), Edinger–Westphal nucleus (EW), and red nucleus (RN) (Fig. 3*A* and *SI Appendix*, Fig. S6). The levels of Piezo1 expression in these brain regions were quantified by their fluorescent intensities and were all found to be greater than in the cortex (Fig. 3*B*). Of these, we were interested in the CEA as a classic and well-established target of neuroscientific experiments controlling defensive and appetitive behaviors (49). To see whether Piezo1 is an important mediator, either in a direct or indirect way, mediating ultrasound neuromodulation in this brain area, a fiber photometry experiment is conducted. Piezo1 expression was knocked out in either neurons or astrocytes of the CEA by viral delivery, and all groups were made to express GCaMP6s (Fig. 3*C*). This enabled the creation of 4 groups, named as follows: "hSyn-Cre" (neuronal P1KO), "hSyn" (neuronal viral Ctrl), "GFAP-Cre" (astrocytic P1KO), and "GFAP" (astrocytic viral Ctrl). Neuronal calcium dynamics in response to ultrasound stimuli were then monitored through fiber photometry in all four groups (*SI Appendix*, Fig. S7). We found a clear, rapid, and consistent increase in GCaMP6s fluorescence to ultrasound pulses of very low intensity (0.12 MPa, 300-ms pulse duration, and 5-s interval) in the hSyn, GFAP, and GFAP-Cre groups but little-to-no response in the hSyn-Cre group (Fig. 3*D*). We did not observe any repetitive patterns of fluorescence changes prior to the US stimulation. The ultrasound parameters used did induce a small Ca^{2+} response in the hSyn-Cre group (0.12 MPa, peak $\Delta F/F_0 = 0.41\% \pm 0.077\%$), but the peak amplitude in the other three groups was significantly higher at same ultrasound intensity (hSyn, $\Delta F/F_0 = 1.13\% \pm 0.17\%$; GFAP-Cre, $\Delta F/F_0 = 1.05\% \pm 0.12\%$; GFAP, $\Delta F/F_0 = 1.12\% \pm 0.10\%$) (Fig. 3 *D* and *E*). Notably, the peak amplitude was found to increase as the applied ultrasound acoustic pressure increased from 0.03 MPa to 0.25 MPa, indicating that the neuronal Ca^{2+} responses were dependent on the amount of ultrasound energy applied (Fig. 3*F*). In all tested cases, the hSyn-Cre group showed significantly lower calcium responses, indicating the importance of neuronal Piezo1 for ultrasound neuromodulation. Since Piezo1 levels were found to be higher in the CEA than in the cortex, we further compared the neuronal responses to ultrasound stimulation between these regions. Quantification of the ΔF/F peaks revealed that the slope of the ΔF/F peak–pressure relation in CEA neurons (k = 4.885) was greater than that of the cortex (k = 1.132) (Fig. 3*G*). Thus, we found that CEA neurons displayed higher Piezo1 expression as well as higher sensitivity to ultrasound compared to the cortex, with acoustic pressures as low as 0.06 to 0.25 MPa. The tunability of the responses to ultrasound parameters also helped to confirm that the observed responses were triggered by ultrasound, and not background signals. These results further confirm that Piezo1 is an important factor mediating ultrasonic neuron modulation in vivo.

Discussion

In this study, we demonstrate that Piezo1 is an important mediator of the ultrasonic neuromodulatory effect to regulate neuronal signaling and animal motor behavior in vivo. We first confirmed the functional expression of Piezo1 in the mouse brain through the generated P1KO mouse model. We found that P1KO neurons displayed lower neuronal activity responding to ultrasound through the reduced ultrasonic motor response, EMG signaling, calcium changes, and c-Fos expression compared to the control. A similar phenomenon was also found in the CEA region; with the knockout of neuronal Piezo1 in the CEA, neurons showed significantly reduced ability to respond to ultrasound. In contrast, CEA neurons, having higher Piezo1 expression levels, displayed greater sensitivity to ultrasound than cortical neurons, showing

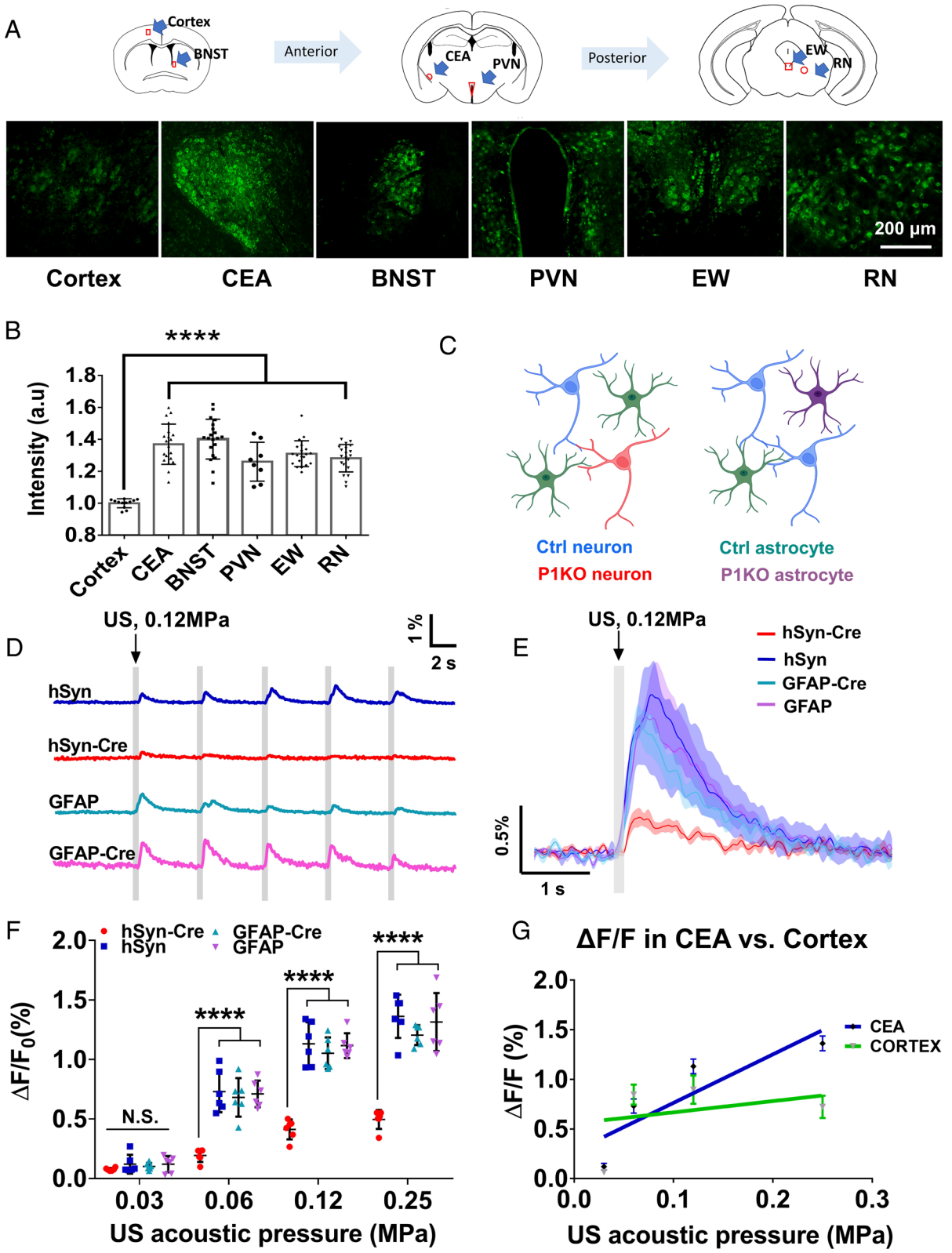

Fig. 3. Neuronal sensitivity to ultrasound stimulation depends on the expression of neuronal Piezo1. (*A*) Immunostaining of Piezo1 in different brain regions, including the cortex, CEA, BNST, PVN, EW, and RN. (*B*) Summarized relative fluorescence intensity of Piezo1 positive cells in different brain areas compared to that in the cortex. Bars represent mean ± SD, ****$P < 0.0001$ by one-way ANOVA followed by Dunnett's multiple comparisons test. (*C*) Schematic illustration of viral treatment in mice to create four groups for fiber photometry, with neuronal or astrocytic P1KO. All groups were injected with hSyn-GCaMP6s. (*D*) Representative calcium response traces under 0.12-MPa ultrasound stimulation in the CEA. (*E*) Representative averaged calcium response traces following one ultrasound stimulus of 0.12 MPa. (*F*) Summarized calcium response to varying ultrasound stimulations. N= 6 mice per viral group. Bars represent mean ± SEM, ****$P < 0.0001$, 'N.S.' not significant by one-way ANOVA with post hoc Tukey's test. Ultrasound parameters were as follows: frequency: 0.5 MHz; duty cycle: 50%, PRF: 1 kHz, duration: 300 ms; 5-s intervals; five times repetition in each intensity group. (*G*) Regression of calcium signal induced by ultrasound in the cortex and CEA from six mice and five mice, respectively. CEAy = 4.885x + 0.2743; cortex: y = 1.132x + 0.5542; slope difference: $P = 0.003388$.

stronger responses at lowered acoustic pressures. We also addressed the auditory confound question by monitoring auditory cortex activation in P1KO and Ctrl mice, as well as applying smoothed waveform ultrasound. Thus, we used a dual approach of comparing neuronal responses to US in the same brain region with Piezo1 knocked out (P1KO vs. Ctrl), and different brain regions with varying Piezo1 levels (CEA vs. Cortex), to demonstrate the contribution of Piezo1 as a mediator of ultrasonic neuromodulation in vivo. Additionally, although we found that Piezo1 expressed in both neurons and astrocytes, we found that neuronal Piezo1 played a major role in mediating ultrasound's effects directly.

While previous studies have identified various mechanosensitive ion channels which respond to ultrasound stimuli in vitro, studies with direct observation in vivo remain limited. It bears repeating that a transgenic animal model with conditional knockout of the ion channel Piezo1 was utilized in this study, allowing precise manipulation of its presence or absence to examine its specific role. We also demonstrated increased response to ultrasound in a region with greater Piezo1 expression. In vivo studies, naturally, provide more realistic scenarios in terms of the cellular/subcellular expression profile of different mechanosensitive ion channels which likely affect their distinct role within a brain network under ultrasound stimulus. We believe that our investigation with a verified KO system, and comparing neurons with differing endogenous levels of Piezo1, in vivo is useful for understanding the mediator roles relevant to ultrasound neuromodulation. These findings add to the literature by demonstrating the potency of ultrasound neuromodulation in the brain even when only endogenous levels of mechanosensitive proteins are involved.

Although the high sensitivity of Piezo1 to sense the mechanical cues (38) may explain its ability to modulate neurons, we also expect that there may be an amplification effect through cooperation with other components. For instance, TRPV4 or SMPD3 may contribute to this Piezo1-mediated ultrasonic neuromodulatory effects through their enhancement in Piezo1 function (50, 51). However, there is no direct evidence demonstrating this hypothesis. We believe that further studies that focus on Piezo1's cooperation with other participants in mechanotransduction under ultrasound stimulation may provide more information about the mechanism.

For the moment, we cannot exclude the role of other cellular machinery since ultrasound neuromodulatory effects were not fully eliminated in the P1KO neurons. Previous studies have shown that some TRP channels such as TRPA1, TRPP1/2, TRPC1, and TRPV1 (35, 37, 52, 53), potassium channels such as TREK1 and TRAAK (34, 54), and calcium voltage-gated channels (55, 56) may also contribute to the ultrasound-induced neural activity. We agree with these findings that other ion channels in different cell types, astrocyte (37) for example, may contribute to ultrasound neuromodulation, especially under high ultrasound acoustic pressure. In the present study, we were able to use low acoustic intensities due to Piezo1's highly mechanosensitive nature. However, at higher intensities, it is understood that other ion channels or mechanotransduction elements, less mechanosensitive than Piezo1, may take over as a coplayer mediating neuromodulation, thus diluting the role of Piezo1. Hence, we believe that under low ultrasound intensity, Piezo1 in neurons is the major mediator mediating the ultrasound neuromodulation in vivo. While our study provides evidence that ultrasound-mediated opening of Piezo1 is a critical mediator of neuromodulation, it remains unclear whether this effect is sufficient to cause action potential generation, which is necessary for the observed animal behavioral changes. To address this limitation, future studies will directly measure the Piezo1-mediated action potential generation in neurons.

An interesting finding slightly orthogonal to the purpose of this study was that we found that Piezo1 was highly expressed in the BNST, CEA, PVN, EW, and RN. These are all corticotropin-releasing factor (CRF)-expressing areas that regulate stress processing in animals (57, 58). CRF is a 41-amino acid peptide which is relatively large compared to other neural transmitters. Neurons might experience more mechanical effects while transporting and secreting this neuron transmitter (56) when processing stress in animals thus requires more Piezo1 in these neurons. However, there is no direct evidence supporting this yet. Nevertheless, with their relatively high expression of Piezo1, ultrasound could provide a way to modulate these neurons to study relevant questions in neuroscience.

Methods

Mice. Animal use and care were performed following the guideline of the Department of Health–Animals (Control of Experiments) of the Hong Kong SAR government. Mice were housed under standard housing conditions with a 12-h light/dark cycle and food and water available ad libitum. Transgenic mice of the lines C57BL6/J (JAX# 000664) and Piezo1$^{tm2.1Apat}$ (JAX# 029213) were maintained for experiments.

Stereotaxic Surgery. Male Piezo1$^{tm2.1Apat}$ mice that were 4 to 8 wk old were deeply anesthetized by 100 mg/mL ketamine and 10 mg/mL xylazine in 0.9% NaCl and positioned in a stereotaxic injection frame (RWD Ltd.). The anesthetized mice were positioned in the stereotaxic apparatus, and ointment was applied on the eyes. Skin incisions were performed to expose the skull. Then, 400 nL of virus was delivered to three locations respectively by a microinjection system (Nanoliter 2010, WPI Ltd.) through a craniotomy (<1 mm^2). The injection was performed unilaterally to the right motor cortex (at mm): AP: 0.0, ML: −1.0; AP: +0.5, ML: −1.0; AP: +0.5, ML: −1.5 with DV: −1. Mice injected with rAAV2/9-Syn-mCherry and rAAV2/9-Syn-Cre-mCherry were "Ctrl" and "P1KO" mice respectively, prepared for behavior, EMG, and c-Fos experiments. Some mice were also simultaneously injected with rAAV2/9-Syn-GCaMP6s to prepare Ctrl and P1KO mice for calcium imaging and FP recordings. The final VG/ml of all viruses was 5×10^{12} VG/mL (all viruses from OBiO Technology). Twenty-four mice were randomly divided into four groups injected with 0.2 μL rAAV-hSyn-GCaMP6s + 0.2 μL pAOV-hSyn-mCherry-2A-Cre / hSyn-mCherry / GFAP-Cre-mCherry / GFAP-mCherry into the CEA area. The coordinates used for the CEA region were AP, −1.22 mm; ML, −2.9 mm; and DV, −4.60 mm.

For mice prepared for the fiber photometry experiments, after finishing the injection, an optic fiber was implanted. The fiber was fixed to the skull with glue and dental cement and was allowed to set for 20 min. Scalp tissue was disinfected, and the mice were moved back to their original housing areas.

Genotyping and Tissue Isolation. The success of conditional knockout was determined by PCR analysis of DNA extracted from brain tissue where the virus was injected. Genotyping was performed according to the protocol as previously specified (45). The following primers were used as indicated in Fig. 1*B*: P1 F: GCC TAG ATT CAC CTG GCT TC; R: GCT CTT AAC CAT TGA GCC ATC T; P1 KO F: CTT GAC CTG TCC CCT TCC CCA TCA AG; R: AGG TTG CAG GGT GGC ATG GCT CTT TTT and Phire II polymerase (Thermo-Scientific #F-170S). PCR was run following the cycling conditions: initial denaturation: 98 °C for 5 min, followed by 98 °C for 5 s, then 10 cycles of 65°C (−0.5°C/cycle) for 5 s, 68°C for 20 s, followed by 30 cycles of 98 °C for 5 s, 60 °C for 5 s, 72 °C for 20 s, followed by a final hold of 72 °C for 1 min. Reactions were separated on 2% agarose gels, yielding the following band sizes: WT, 188 bp; P1, 380 bp; and P1KO, 230 bp.

Calcium Imaging Ex Vivo. Mice were deeply anesthetized by intraperitoneal injection of ketamine/xylazine mixture (100 mg/kg and 10 mg/kg body weight) and transcranially perfused with NMDG aCSF containing 92 mM NMDG, 2.5mM KCl, 1.25mM NaH_2PO_4, 20mM $NaHCO_3$, 10mM HEPES, 25 mM glucose, 2 mM thiourea, 5 mM Na-ascorbate, 3 mM Na-pyruvate, 0.5 mM $CaCl_2{\cdot}4H_2O$, 10 mM $MgSO_4{\cdot}7H_2O$, and 12 mM NAC (pH titrated to 7.3 to 7.4 with concentrated HCl). Coronal brain sections 300 to 400-μm thick were cut with a vibratome (Leica, VT1000S) in ice-cold NMDG aCSF. Slices were recovered for 10 to 12 min at

32°C in NMDG aCSF. After that, slices were recovered in HEPES aCSF containing 92 mM NaCl, 2.5 mM KCl, 1.25 mM NaH_2PO_4, 30 mM $NaHCO_3$, 20 mM HEPES, 25 mM glucose, 2 mM thiourea, 5 mM Na-ascorbate, 3 mM Na-pyruvate, 2 mM $CaCl_2{\cdot}4H_2O$, and 2 mM $MgSO_4{\cdot}7H_2O$ at room temperature for at least 1 h. The slice was then transferred to the recording ACSF (rACSF) perfusing confocal dish for the calcium image. The rACSF contained 126 mM NaCl, 1.6 mM KCl, 1.2 mM NaH_2PO_4, 1.2 mM $MgCl_2$, 2.4 mM $CaCl_2$, 18 mM $NaHCO_3$, and 11 mM glucose. All aCSF solutions were saturated with carbogen (95% O_2 /5% CO_2) prior to use to ensure stable pH buffering and adequate oxygenation. A 0.5-MHz plane transducer was placed in a handmade tube, which allowed control of the stimulation area to 4 mm^2 and was adjusted into a position underneath the rACSF confocal dish. Ultrasound stimuli (0.35 MPa) were administered with 500-μs tone burst, 1-kHz PRF, and 300-ms duration. The fluorescence change indicated by GCaMP6s fluorescence intensity was calculated by $\Delta F/F_0 = (F-F0)/F0$, taking F_0 to be the baseline of the fluorescence signal averaged over 10 to 50 s before the ultrasound onset in each session. Quantification and calculations for these experiments were performed by an experimenter blinded to the identity of the groups.

Video Capture of Limb Movements. Both video capture and EMG experiments were conducted after 4 to 6 wk of viral injection. Under isoflurane/O_2 anesthesia, the mice's heads were shaved, and a 0.5-MHz lithium niobate ultrasound transducer was coupled to the skull using ultrasound gel (Parker Aquasonic 100). For video-capturing, 0.35/0.45-MPa ultrasound stimuli were administered with 500-μs tone burst, 1-kHz PRF, 50/250/500-ms duration, and 5-s intervals. The experimenter performing the US stimulation was blinded to which group the animal belonged. Videos were captured at a rate of 30 Hz, which was later analyzed by an open-source machine learning toolkit for animal pose estimation DeepLabCut. Forelimb and hind limb trajectories after ultrasound stimulation were calculated. The greatest movements of forelimb and hind limb digital ends within 3 s after ultrasound stimuli were extracted in terms of distance away from the position when the corresponding ultrasound stimulus was applied. For behavioral tests in mice that were stimulated in either ipsilateral or contralateral hemispheres, the experimental parameters were kept the same, except for the ultrasound waveform being smoothed through an ultrasound modulator, and the pluses were triggered randomly (RIGOL, DG1032).

EMG Experiments. For EMG experiments, ultrasound stimuli (0.3, 0.35, 0.4, and 0.45 MPa) were administered with 500-μs tone burst, 1-kHz PRF, 500-ms duration, and 15-s intervals. EMG data were collected from the left gastrocnemius muscle through fine needle electrodes connected to a Meduda (Bio-Signal Technology). Data were recorded at 1,000 Hz, preamplified, and digitized. Using MATLAB (MathWorks), digitized waveforms were filtered by a 50-Hz notch filter and a 300-Hz high-pass filter. Root-mean-square envelopes of the filtered waveforms were extracted for EMG identification and feature extraction. After smoothing the envelope, mean amplitude of 'quiet period' prior any ultrasound stimulation was taken as baseline. If any peak rose above four times the baseline within the 1-s window after US stimulation onset, whose waveform remained lower than two times the baseline within a 300-ms window prior to the onset of stimulation, the peak was considered a successful US-induced EMG response and the amplitude was extracted.

Fiber Photometry. Following implantation and recovery, around 4 wk, mice were anesthetized with isoflurane (1.0 to 2.5% in O_2). Ultrasound gel was applied on a shaved head, to promote acoustic coupling. A 0.5-MHz transducer embedded with a water tube wave-guide was installed above the skull. Mice were stimulated with four trials of ultrasound stimulation (0.03 MPa, 0.06 MPa, 0.12 MPa, or 0.25 MPa). Each trial was three to six ultrasound stimuli, with a 5-s interval between each pulse. Mice were allowed to rest for 50 s between trials. GCaMP6s fluorescence was captured with a fiber photometry system (Thinker Tech Nanjing BioScience Inc.). The excitation and receiving wavelengths for fiber photometry were 470 nm with 30 nm bandwidth and 510 nm with 25 nm bandwidth, respectively. Data were collected at 100 Hz and analyzed using a customized MATLAB script. The relative change in fluorescence, $\Delta F/F_0 = (F-F0)/F0$, was calculated by taking F_0 to be the baseline of the fluorescence signal averaged over 1 s before the ultrasound onset in each session.

Immunohistochemical Fluorescent Staining. Mice were killed 90 min after ultrasound treatment and perfused with phosphate-buffered saline (PBS, 0.01 M, pH 7.4), followed by 4% paraformaldehyde (PFA) (cat. no. P1110, Solarbio) in PBS. After dissection, brains were postfixed overnight in 4% PFA and then rinsed in PBS. Starting from the injection plane, around 10 continuous coronal brain slices with an interval of 105 μm were collected. Slices were blocked using a blocking medium containing 10% normal goat serum, 1% bovine serum albumin, and 0.3% Triton X-100, for 90 min and incubated overnight in a primary antibody solution diluted in blocking. Slices were then washed and incubated with secondary antibodies diluted in PBS for 90 min at room temperature. Slices were then washed, stuck to glass slides, dried, and mounted on coverslips using small drops of Prolong Diamond Antifade Mountant with DAPI and allowed to cure in the dark at room temperature overnight. Coverslip edges were sealed using transparent nail enamel and imaged using a confocal laser scanning microscope (TCS SP8, Leica). Primary antibodies used were c-Fos (2250, CST, dilution 1:500), Piezo1 (ab128245, Abcam, dilution 1:50), and MAP2 (PA1-16751, Invitrogen, dilution 1:500). For the blocking experiments, specific Piezo1 immunizing peptide (ab133015, Abcam, concentration: 20 μg/mL) was added to the Piezo1 antibody for 2 h preincubation. Secondary antibodies, used at a dilution of 1:1,000, were goat anti-rabbit IgG (H+L) Alexa Fluor 488 (A-11008, Invitrogen) and goat anti-mouse IgY (H+L) Alexa Fluor 633 (A-21103, Invitrogen). The number of c-Fos (green)-stained neurons in 853 × 853 μm slice was counted using ImageJ. The counting was single-blinded, performed by an experimenter who did not know the groups beforehand.

Statistics. Statistical analyses were performed in GraphPad Prism. All statistical tests in this study were two tailed. Single-variable comparisons were made with the *t* test. Group comparisons were made using either ANOVA followed by Tukey's post hoc analysis, Holm-Sidak's test, or Dunnett's test.

Data, Materials, and Software Availability. The data have been deposited in the Figshare repository (https://figshare.com/articles/dataset/Zhu_et_al_2023_data_files/22631044) (59). All other study data are included in the article and/or *SI Appendix*.

ACKNOWLEDGMENTS. This work was supported by the Guangdong High Level Innovation Research Institute (2021B0909050004), the Hong Kong Research Grants Council General Research Fund (15104520, 15102417, and 15326416), Hong Kong Innovation Technology Fund (MRP/018/18X and MHP/014/19), Shenzhen-Hong Kong Macaus Science and Technology Program (Category C), Key-Area Research and Development Program of Guangdong Province (2018B030331001), internal funding from the Hong Kong Polytechnic University Research Institute of Smart Ageing (1-CD76), and Hong Kong Polytechnic University (1-ZE1K, 1-BBAU, and 1-ZVW8). We would like to thank the facility and technical support from University Research Facility in Life Sciences and University Research Facility in Behavioral and Systems Neuroscience of The Hong Kong Polytechnic University.

Author affiliations: [a]Department of Biomedical Engineering, The Hong Kong Polytechnic University, Hong Kong SAR 999077, China; and [b]Guangdong Institute of Intelligence Science and Technology, Hengqin, Zhuhai, Guangdong 519031, China

1. W. Legon *et al.*, Transcranial focused ultrasound modulates the activity of primary somatosensory cortex in humans. *Nat. Neurosci.* **17**, 322–329 (2014).
2. W. Lee *et al.*, Image-guided transcranial focused ultrasound stimulates human primary somatosensory cortex. *Sci. Rep.* **5**, 1–10 (2015).
3. W. Legon, L. Ai, P. Bansal, J. K. Mueller, Neuromodulation with single-element transcranial focused ultrasound in human thalamus. *Hum. Brain Mapp.* **39**, 1995–2006 (2018).
4. W. Lee *et al.*, Transcranial focused ultrasound stimulation of human primary visual cortex. *Sci. Rep.* **6**, 34026 (2016).
5. W. Legon, P. Bansal, R. Tyshynsky, L. Ai, J. K. Mueller, Transcranial focused ultrasound neuromodulation of the human primary motor cortex. *Sci. Rep.* **8**, 1–14 (2018).
6. J. L. Sanguinetti *et al.*, Transcranial focused ultrasound to the right prefrontal cortex improves mood and alters functional connectivity in humans. *Front. Hum. Neurosci.* **14**, 52 (2020).
7. S. J. Reznik, J. L. Sanguinetti, W. J. Tyler, C. Daft, J. J. Allen, A double-blind pilot study of transcranial ultrasound (TUS) as a five-day intervention: TUS mitigates worry among depressed participants. *Neurol. Psychiatry Brain Res.* **37**, 60–66 (2020).
8. J. A. Cain *et al.*, Ultrasonic thalamic stimulation in chronic disorders of consciousness. *Brain Stimulation: Basic, Translational, and Clinical Research in Neuromodulation* **14**, 301–303 (2021).
9. Y. Tufail *et al.*, Transcranial pulsed ultrasound stimulates intact brain circuits. *Neuron* **66**, 681–694 (2010).

10. S. S. Yoo *et al.*, Focused ultrasound modulates region-specific brain activity. *Neuroimage* **56**, 1267–1275 (2011).
11. H. Kim *et al.*, Noninvasive transcranial stimulation of rat abducens nerve by focused ultrasound. *Ultrasound Med. Biol.* **38**, 1568–1575 (2012).
12. R. L. King, J. R. Brown, W. T. Newsome, K. B. Pauly, Effective parameters for ultrasound-induced in vivo neurostimulation. *Ultrasound Med. Biol.* **39**, 312–331 (2013).
13. R. L. King, J. R. Brown, K. B. Pauly, Localization of ultrasound-induced in vivo neurostimulation in the mouse model. *Ultrasound Med. Biol.* **40**, 1512–1522 (2014).
14. P. P. Ye, J. R. Brown, K. B. Pauly, Frequency dependence of ultrasound neurostimulation in the mouse brain. *Ultrasound Med. Biol.* **42**, 1512–1530 (2016).
15. K. Yu, X. Niu, E. Krook-Magnuson, B. He, Intrinsic functional neuron-type selectivity of transcranial focused ultrasound neuromodulation. *Nat. Commun.* **12**, 2519 (2021).
16. W. Lee *et al.*, Image-guided focused ultrasound-mediated regional brain stimulation in sheep. *Ultrasound Med. Biol.* **42**, 459–470 (2016).
17. T. Deffieux *et al.*, Low-intensity focused ultrasound modulates monkey visuomotor behavior. *Curr. Biol.* **23**, 2430–2433 (2013).
18. N. Wattiez *et al.*, Transcranial ultrasonic stimulation modulates single-neuron discharge in macaques performing an antisaccade task. *Brain stimul.* **10**, 1024–1031 (2017).
19. G. Ter Haar, Therapeutic applications of ultrasound. *Progress Biophys. Mol. Biol.* **93**, 111–129 (2007).
20. C. Iorio-Morin *et al.*, Bilateral focused ultrasound thalamotomy for essential tremor (BEST-FUS phase 2 trial). *Movement Disorders* **36**, 2653–2662 (2021).
21. A. Sinai *et al.*, Focused ultrasound thalamotomy in tremor dominant Parkinson's disease: Long-term results. *J. Parkinson's Dis.* **12**, 199–206 (2022).
22. J. Germann *et al.*, Potential optimization of focused ultrasound capsulotomy for obsessive compulsive disorder. *Brain* **144**, 3529–3540 (2021).
23. M. Dinno *et al.*, The significance of membrane changes in the safe and effective use of therapeutic and diagnostic ultrasound. *Phys. Med. Biol.* **34**, 1543 (1989).
24. D. Dalecki, Mechanical bioeffects of ultrasound. *Annu. Rev. Biomed. Eng.* **6**, 229–248 (2004).
25. W. D. O'Brien Jr., Ultrasound–biophysics mechanisms. *Progress Biophys. Mol. Biol.* **93**, 212–255 (2007).
26. H. Kim, A. Chiu, S. D. Lee, K. Fischer, S. S. Yoo, Focused ultrasound-mediated non-invasive brain stimulation: examination of sonication parameters. *Brain Stimul.* **7**, 748–756 (2014).
27. W. J. Tyler, S. W. Lani, G. M. Hwang, Ultrasonic modulation of neural circuit activity. *Curr. Opin. Neurobiol.* **50**, 222–231 (2018).
28. J. Kubanek, P. Shukla, A. Das, S. A. Baccus, M. B. Goodman, Ultrasound elicits behavioral responses through mechanical effects on neurons and ion channels in a simple nervous system. *J. Neurosci.* **38**, 3081–3091 (2018).
29. T. G. Leighton, What is ultrasound? *Prog. Biophys. Mol. Biol.* **93**, 3–83 (2007).
30. M. D. Menz *et al.*, Radiation force as a physical mechanism for ultrasonic neurostimulation of the ex vivo retina. *J. Neurosci.* **39**, 6251–6264 (2019).
31. A. Fomenko, C. Neudorfer, R. F. Dallapiazza, S. K. Kalia, A. M. Lozano, Low-intensity ultrasound neuromodulation: An overview of mechanisms and emerging human applications. *Brain Stimul.* **11**, 1209–1217 (2018).
32. J. Kubanek *et al.*, Ultrasound modulates ion channel currents. *Sci. Rep.* **6**, 24170 (2016).
33. Z. Qiu *et al.*, The mechanosensitive ion channel piezo1 significantly mediates in vitro ultrasonic stimulation of neurons. *iScience* **21**, 448–457 (2019).
34. B. Sorum, R. A. Rietmeijer, K. Gopakumar, H. Adesnik, S. G. Brohawn, Ultrasound activates mechanosensitive TRAAK K+ channels through the lipid membrane. *Proc. Natl. Acad. Sci. U.S.A.* **118**, e2006980118 (2021).
35. S. Yoo, D. R. Mittelstein, R. C. Hurt, J. Lacroix, M. G. Shapiro, Focused ultrasound excites cortical neurons via mechanosensitive calcium accumulation and ion channel amplification. *Nat. Commun.* **13**, 493 (2022).
36. Z. Qiu *et al.*, Targeted neurostimulation in mouse brains with non-invasive ultrasound. *Cell Rep.* **32**, 108033 (2020).
37. S. J. Oh *et al.*, Ultrasonic neuromodulation via Astrocytic TRPA1. *Curr. Biol.* (2019), 10.1016/j.cub.2019.08.021.
38. B. Coste *et al.*, Piezo1 and Piezo2 are essential components of distinct mechanically activated cation channels. *Science* **330**, 55–60 (2010).
39. J. Wu, R. Goyal, J. Grandl, Localized force application reveals mechanically sensitive domains of Piezo1. *Nat. Commun.* **7**, 12939 (2016).
40. F. Falleroni *et al.*, Mechanotransduction in hippocampal neurons operates under localized low picoNewton forces. *iScience* **25**, 103807 (2022).
41. E. S. Lein *et al.*, Genome-wide atlas of gene expression in the adult mouse brain. *Nature* **445**, 168–176 (2007).
42. E. Sjöstedt *et al.*, An atlas of the protein-coding genes in the human, pig, and mouse brain. *Science* **367**, eaay5947 (2020).
43. L. J. Drew, J. N. Wood, P. Cesare, Distinct mechanosensitive properties of capsaicin-sensitive and-insensitive sensory neurons. *J. Neurosci.* **22**, RC228-RC228 (2002).
44. C. Aurup, H. A. S. Kamimura, E. E. Konofagou, High-resolution focused ultrasound neuromodulation induces limb-specific motor responses in mice in vivo. *Ultrasound Med. Biol.* **47**, 998–1013 (2021).
45. S. M. Cahalan *et al.*, Piezo1 links mechanical forces to red blood cell volume. *Elife* **4**, e07370 (2015).
46. H. Guo *et al.*, Ultrasound produces extensive brain activation via a cochlear pathway. *Neuron* **98**, 1020–1030.e1024 (2018).
47. T. Sato, M. G. Shapiro, D. Y. Tsao, Ultrasonic neuromodulation causes widespread cortical activation via an indirect auditory mechanism. *Neuron* **98**, 1031–1041.e1035 (2018).
48. M. Mohammadjavadi *et al.*, Elimination of peripheral auditory pathway activation does not affect motor responses from ultrasound neuromodulation. *Brain Stimul.* (2019), 10.1016/j.brs.2019.03.005.
49. J. P. Fadok, M. Markovic, P. Tovote, A. Lüthi, New perspectives on central amygdala function. *Curr. Opin. Neurobiol.* **49**, 141–147 (2018).
50. S. M. Swain, R. A. Liddle, Piezo1 acts upstream of TRPV4 to induce pathological changes in endothelial cells due to shear stress. *J. Biol. Chem.* **296,** 100171 (2021).
51. J. Shi *et al.*, Sphingomyelinase disables inactivation in endogenous PIEZO1 channels. *Cell Rep.* **33**, 108225 (2020).
52. S. R. Burks, R. M. Lorsung, M. E. Nagle, T.-W. Tu, J. A. Frank, Focused ultrasound activates voltage-gated calcium channels through depolarizing TRPC1 sodium currents in kidney and skeletal muscle. *Theranostics* **9**, 5517 (2019).
53. Y. Yang *et al.*, Sonothermogenetics for noninvasive and cell-type specific deep brain neuromodulation. *Brain Stimul.* **14**, 790–800 (2021).
54. M. Lengyel, P. Enyedi, G. Czirják, Negative influence by the force: Mechanically induced hyperpolarization via k2p background potassium channels. *Int. J. Mol. Sci.* **22**, 9062 (2021).
55. J. Arnadottir, M. Chalfie, Eukaryotic mechanosensitive channels. *Annu. Rev. Biophys.* **39**, 111–137 (2010).
56. W. J. Tyler, The mechanobiology of brain function. *Nat. Rev. Neurosci.* **13**, 867–878 (2012).
57. S. M. Smith, W. W. Vale, The role of the hypothalamic-pituitary-adrenal axis in neuroendocrine responses to stress. *Dialogues Clin. Neurosci.* **8**, 383–395 (2022).
58. M. J. Henckens, J. M. Deussing, A. Chen, Region-specific roles of the corticotropin-releasing factor–urocortin system in stress. *Nat. Rev. Neurosci.* **17**, 636–651 (2016).
59. J. Zhu *et al.*, 2023 data files. Figshare. https://figshare.com/articles/dataset/Zhu_et_al_2023_data_files/22631044. Deposited 14 April 2023.